

Carbon formation in catalytic partial oxidation of methane on platinum: Model studies on a polycrystalline Pt foil¹

Abstract

A polycrystalline Pt foil has been investigated as model catalyst in methane catalytic partial oxidation to synthesis gas. It is demonstrated that a substantial amount of carbonaceous deposits forms on the Pt foil upon reaction light-off blocking a large fraction of Pt surface atoms. By using in situ Raman spectroscopy and quantitative spectral analysis the evolution and spatial distribution of these carbonaceous compounds with reaction temperature and reaction time have been characterized. The chemical composition of the carbon material changes from highly reactive and strongly disordered directly after reaction light-off to highly ordered, oxidation and steam reforming resistant after several hours time on stream at 800 °C reaction temperature. Remarkably the carbon distribution at the Pt surface was found to be inhomogeneous and related to the nature of the microcrystals forming the polycrystalline foil in a yet unknown manner.

Keywords

Catalytic partial oxidation, Methane, Synthesis gas, Platinum, Carbon, Raman spectroscopy

1 Introduction

The catalytic partial oxidation (CPO) of methane (Eq. 1) is a potential technology for decentralized conversion of natural gas, consisting mainly of methane, into synthesis gas or hydrogen. In comparison to industrial synthesis gas production by highly endothermic steam reforming (Eq. 2) carried out in large and cost-intensive tube furnaces, methane CPO is exothermic and can produce synthesis gas yields close to thermodynamic equilibrium in millisecond contact times if proper catalysts are chosen. Due to the high rate and exothermicity, technical CPO reactors could be much smaller than steam reformers and could operate adiabatically as the reaction is self sustained and high temperatures favor synthesis gas production over total oxidation (Eq. 3).



Hickman and Schmidt [1–4] showed that Pt and Rh supported on highly porous α -alumina foam monoliths (porosity > 80 %) make excellent CPO catalysts due to their low pressure drop at outstanding transport characteristics.

By means of spatial reactor profiles it was later shown by Horn et al. [5] that on both Rh and Pt coated foam catalysts syngas formation can be formally described by a combined oxidation (Eq. 4) and steam reforming (Eq. 2) mechanism. Dry (CO₂) reforming, as sometimes reported in the literature, is not observed [6].

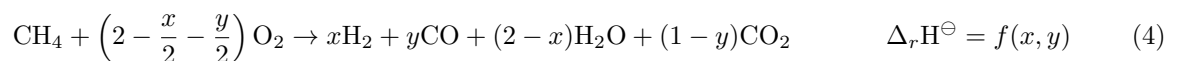


Fig. 1 shows a comparison of spatial profiles measured in Rh and Pt foam catalysts for a stoichiometric CH₄/O₂ ratio according to Eq. 1 reproduced from [5] with permission by Elsevier. These profiles were measured at exactly equal conditions (equal metal loading, equal reactant stoichiometry, equal flow rate, equal support) reflecting the difference in the catalytic performance of Rh and Pt. It can be seen that even though species and temperature develop similarly in both foam catalysts quantitative differences exist leading to an overall lower methane conversion and lower syngas selectivity at the end of the Pt foam catalyst compared to the Rh foam catalyst ($X_{\text{CH}_4}^{\text{Rh}} = 76\%$, $X_{\text{CH}_4}^{\text{Pt}} = 62\%$, $S_{\text{H}_2}^{\text{Rh}} = 96\%$, $S_{\text{H}_2}^{\text{Pt}} = 65\%$, $S_{\text{CO}}^{\text{Rh}} = 92\%$, $S_{\text{CO}}^{\text{Pt}} = 73\%$).

While it was demonstrated experimentally [7] and numerically [8–10] for Rh foam catalysts that methane CPO is film transport limited under basically all investigated conditions, it was found that methane CPO

¹Adapted from O. Korup, R. Schlögl, R. Horn *Catal. Today* 181 (1) (2012) 177-183.

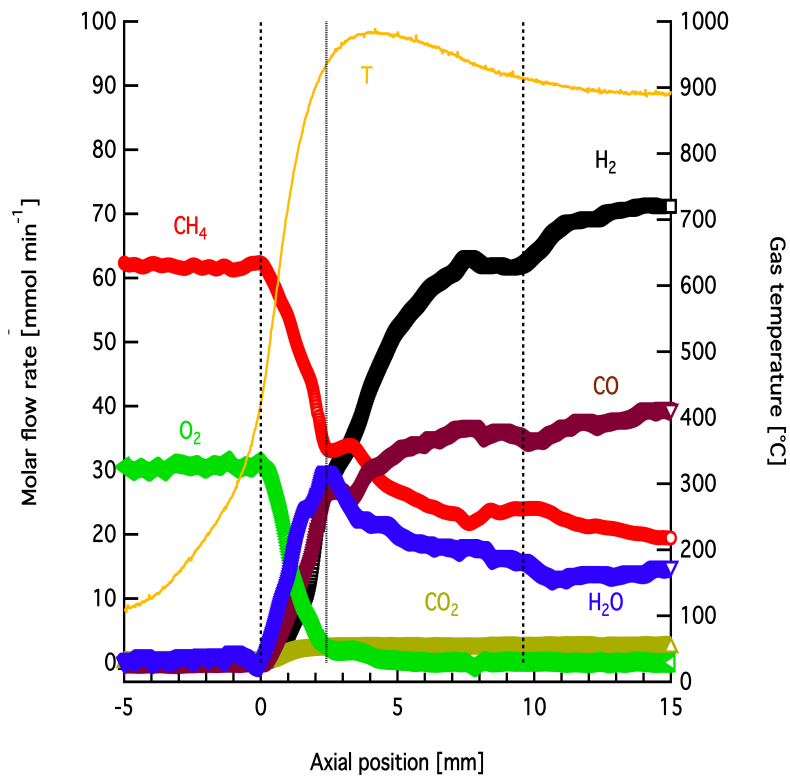
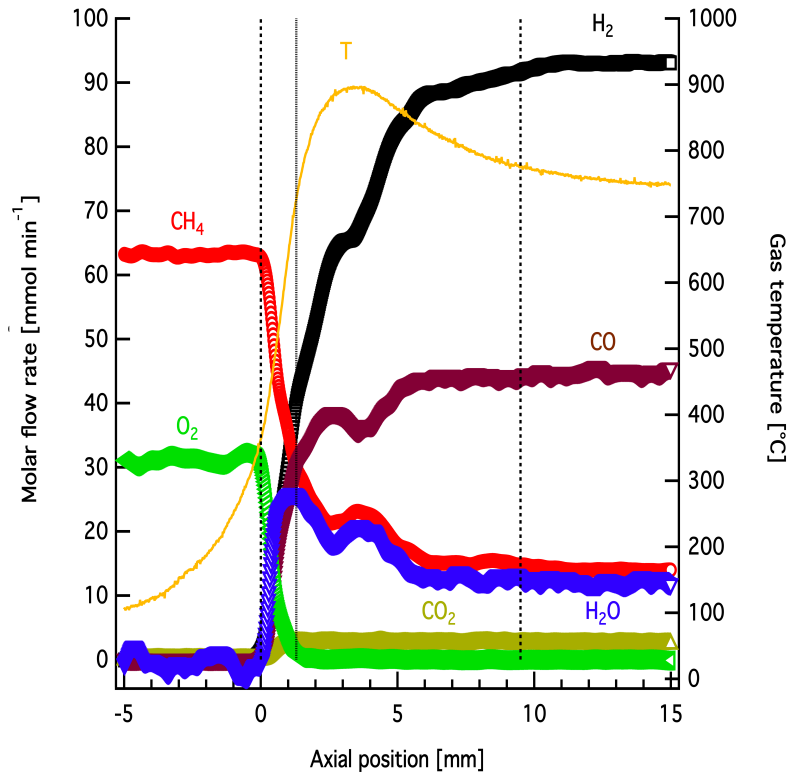


Figure 1: Comparison of two spatially resolved species and gas phase temperature profiles for methane CPO on rhodium and platinum. Top: 5 wt% Rh supported on an 80 ppi α -alumina foam monolith of about ~ 10 mm length. Bottom: 5 wt% Pt supported on an analog foam monolith. Total inlet gas feed in both cases $\dot{V}_{\text{CH}_4} + \dot{V}_{\text{O}_2} + \dot{V}_{\text{Ar}} = 4700 \text{ mln min}^{-1}$ at 273 K. Inlet stoichiometry $\text{C/O} = \dot{V}_{\text{CH}_4}/(2 \cdot \dot{V}_{\text{O}_2}) = 1.0$ and $\dot{V}_{\text{Ar}}/\dot{V}_{\text{O}_2} = 3.76$. Catalyst foam between first and last dotted line. Length of oxidation zone indicated by second dotted line. Data reproduced from [5] with permission by Elsevier.

on Pt foam catalysts is largely kinetically controlled [5,7]. Indeed it is clearly seen in Fig. 1 that reactant conversion and product formation is much slower on the Pt foam catalyst than on the Rh foam catalyst and the question arises why this is the case.

Giving an answer to this question is of considerable interest not only from a fundamental but also from a practical point of view because it could be that the superior catalytic performance of the Rh foam catalyst in terms of methane conversion and synthesis gas selectivity is solely due to the higher reaction rate leading to pronounced film transport limitation and a very low O₂ concentration at the Rh surface as it was numerically predicted by Dalle Nogare et al. [8]. In this case all surface reactions would proceed at the highest physically possible rate, viz. the rate of species transport to the Rh surface, leading to high methane conversion in the oxidation and steam reforming zone (Fig. 1). In terms of syngas selectivity a low O₂ concentration at the Rh surface leads to high selectivity to partial oxidation products already at the end of the oxidation zone which is then further improved by rapid steam reforming in the steam reforming zone.

This more physical explanation shines a new light onto the selectivity discussion given in the landmark paper by Hickman and Schmidt [1] where the poorer performance of Pt compared to Rh was attributed solely to a difference in the activation barrier for the surface reaction $H^* + O^* \rightarrow OH^*$ of $E_a^{Pt} = 20 \text{ kcal mol}^{-1}$ vs. $E_a^{Rh} = 2.5 \text{ kcal mol}^{-1}$, respectively. It is in fact rather unlikely that such differences in activation barriers have a pronounced influence at temperatures close to 1000 °C and in presence of pronounced film transport limitations such as on Rh.

In the present paper we demonstrate that oxidation and steam reforming resistant carbon deposits form on a Pt surface upon ignition of methane oxidation blocking a large fraction of Pt surface atoms. This observation, even though obtained on a polycrystalline Pt foil as a model system and not yet reproduced for a Pt coated foam catalyst, could be a tentative explanation why methane oxidation and methane steam reforming is significantly slower on Pt compared to Rh with all the catalytic consequences outlined above.

2 Experimental

All experiments were conducted in a temperature controlled in situ reactor cell (Linkam Scientific Instruments, type CCR1000) located under a confocal Raman microscope. The reactor was operated at 1atm pressure and could be heated up to 1000 °C using a pre-defined temperature program monitored by a thermocouple in direct thermal contact with the reactor sample holder.

A high purity platinum foil was used as model catalyst (Goodfellow Cambridge Limited, 99.99+ % purity, polycrystalline $\sim 4 \text{ mm} \times 4 \text{ mm} \times 0.125 \text{ mm}$) mounted on the inner rim of the reactors virtually unreactive ceramic crucible. The platinum foil was cleaned prior to the experiments by repeated rinsing in diluted nitric acid. After placing the foil in the reactor cell it was further cleaned by oxidation at 800 °C (30 min, 20 vol.% O₂ in Ar, 50 mln min⁻¹) followed by reduction at the same temperature (30 min, 20 vol.% H₂ in Ar, 50 mln min⁻¹) and cooling down to room temperature.

Online gas analytics was accomplished by a calibrated mass spectrometer (Pfeiffer Vacuum) in analog scan mode using the Ar peak at $m/z = 40$ as internal standard.

Raman spectra were recorded by a triple filter Raman spectrometer (TriVista S&I GmbH) with a CCD camera (Princeton Instruments) as detector attached to a confocal microscope (Olympus, 10x long-working distance objective), using an Ar⁺ laser with $\lambda_0 = 488 \text{ nm}$ excitation wavelength (3 mW on the sample). The spectrometer was operated in triple subtractive mode and each spectrum was integrated for 10 min. A two point wavelength calibration was used (laser wavelength and first-order Stokes phonon band of Si at 520 cm⁻¹).

At the applied laser wavelength of 488 nm an intense continuum background occurs at temperatures above 600 °C due to black body radiation from the sample. To overcome this problem an algorithm developed by Gornushkin et al. [11] was adapted to automatically eliminate the continuum background without significantly compromising the spectral integrity in the region of interest². An exemplary spectrum of untreated raw data (black trace), estimated black body background (red trace) and corrected spectrum (blue trace) is depicted in Fig. 2. For better comparability the baseline corrected spectra were normalized to the G band intensity and fitted depending on the general peak shape. Two cases can be discriminated as shown in Fig.3. Baseline separated peaks are fitted by two Lorentzian-shaped bands with maxima at about $\sim 1350 \text{ cm}^{-1}$ (D band) and $\sim 1580 \text{ cm}^{-1}$ (G band) (Fig. 3, top panel). If two broad and overlapping Raman bands occur they are fitted by the five peak method proposed by Sadezky et al. [12]. These authors suggest a combination of four Lorentzian-shaped bands labeled D4, D1, G, and D2 centered around 1200, 1350, 1580, and 1620 cm⁻¹ respectively, and one Gaussian-shaped D3 band centered around 1500 cm⁻¹. For spectral analysis the Stokes shift band position, full width at half maximum (FWHM), and integrated band intensity were determined from the spectra.

²The correction was accomplished in two steps by a MATLAB script, which is exemplified in appendix ??.

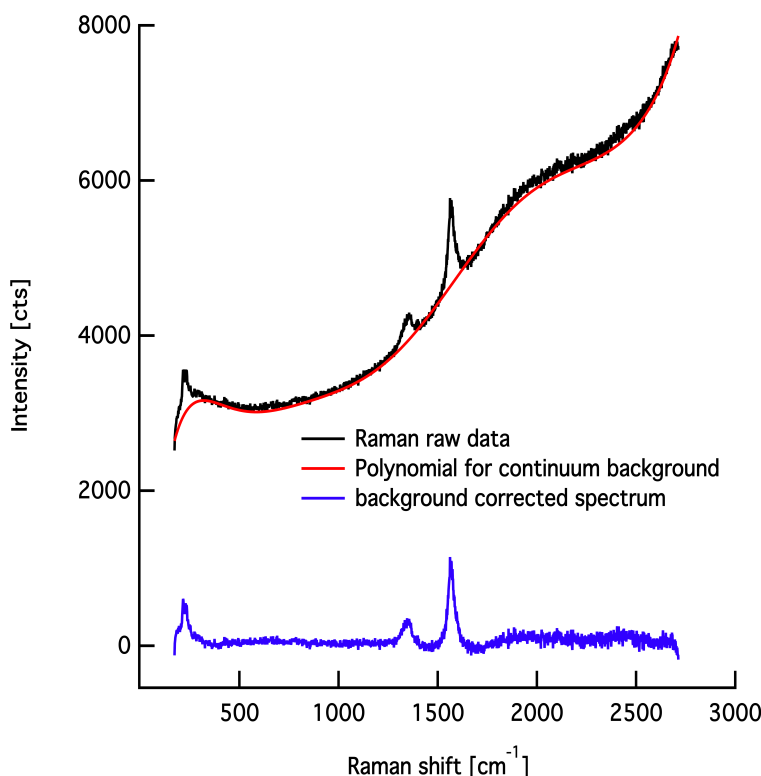


Figure 2: Background correction of in-situ Raman spectra of carbonaceous deposits on a platinum foil during CPO of methane recorded at 800 °C reactor temperature. Black: Raman raw data, Red: estimated polynomial for continuum background by black body radiation from the sample adapted from Gornushkin et al. [11] and Blue: background corrected Raman spectrum.

3 Results and Discussion

3.1 Raman Spectra of Defective Carbon

The first-order Raman spectra of disordered and amorphous carbonaceous materials such as coke or soot are characterized by two broad and usually overlapping peaks with maxima at around $\sim 1350 \text{ cm}^{-1}$ (D peak) and $\sim 1580 \text{ cm}^{-1}$ (G peak). The G or ‘graphite’ peak is attributed to the vibrational mode of in-plane bond stretching motion of sp^2 -hybridized carbon atoms with E_{2g} symmetry in an ideal graphitic lattice [13]. The D or ‘defect’ bands are characteristic for disordered graphite. Their intensity relative to the G peak increases with increasing degree of disorder [14]. The D bands are attributed in literature as follows: The intense D1 band, which is located at about $\sim 1350 \text{ cm}^{-1}$ is associated with the A_{1g} breathing mode of a graphitic lattice. It is assigned to carbon atoms adjacent to lattice disturbance such as graphene layer edges [12,14–16] or a hetero atom in the case of doped graphite [12,16]. The D1 FWHM exhibits a nearly linear negative correlation with the amount of apparent elemental carbon in carbonaceous materials [17,18]. The shoulder of the D1 band at about $\sim 1200 \text{ cm}^{-1}$, usually referred to as D4, is assigned to sp^2 - sp^3 bonds or C–C or C=C stretching vibrations of polyene-like structures with A_{1g} symmetry [12,19,20]. The signal intensity between the two main features of the carbon signal is assigned to an additional band D3 located at about $\sim 1500 \text{ cm}^{-1}$. The D3 band originates from amorphous carbon species, viz. organic molecules, fragments, and functional groups, on interstitial places in the disturbed graphitic lattice of soot [12,19–22]. For soot and related carbonaceous materials it has been shown that the D3 band intensity together with the D1 band FWHM allow to derive information about the relative abundance and structural order of graphite-like and molecular carbon [12,18]. These spectroscopic parameters give most information on amorphisation/graphitization of a certain carbon material. Finally the G band around $\sim 1580 \text{ cm}^{-1}$ is also suggested to be a superposition of two bands in which the additional band at $\sim 1620 \text{ cm}^{-1}$ is referred to as D2 band. The D2 band was assigned to a lattice vibration analogous to the G band but involving vibrations of surface graphene layers [12,16].

3.2 In-situ Raman Spectra During Temperature Programmed Reaction

A temperature programmed experiment with nine temperature steps from room temperature to 800 °C reactor temperature was performed to investigate the existence and nature of carbon deposits forming on

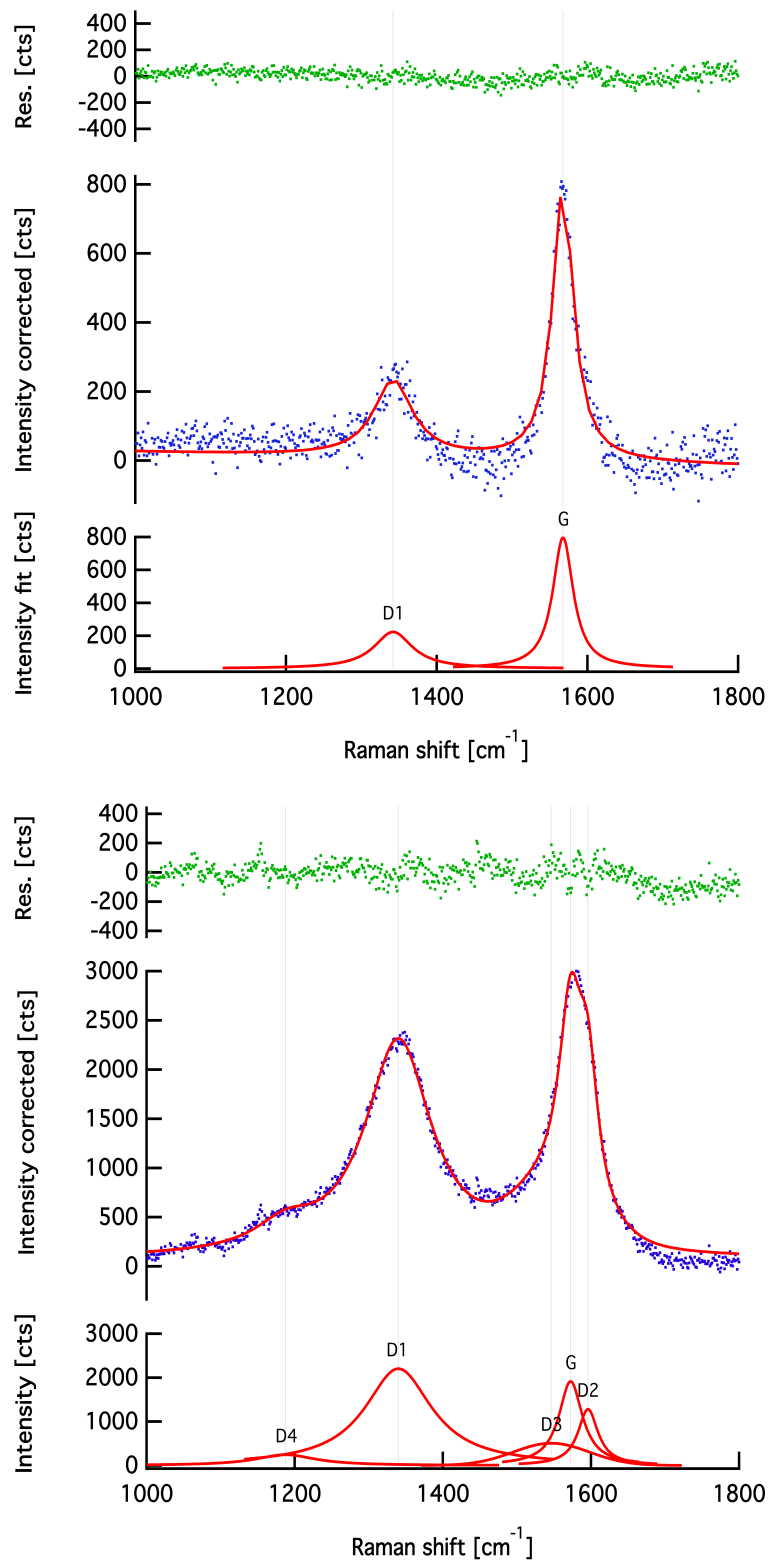


Figure 3: Top: Fit of two baseline separated carbon peaks by two Lorentzian-shaped bands [13]. Bottom: Fit of two broad overlapping peaks by combination of four Lorentzian-shaped and one Gaussian-shaped bands after Sadezky et al. [12].

platinum during methane CPO. The Raman sampling position was chosen arbitrarily close to position 24 in a region with less scratch marks from cut and handling as indicated in Fig. 4. At a constant gas feed rate of composition $\dot{V}_{Ar}/\dot{V}_{CH_4}/\dot{V}_{O_2} = 8.94/5.81/2.41 \text{ mln min}^{-1}$ respectively ($C/O = 1.2$), the reactor cell was stepwise heated (heating rate 50 K min^{-1}) starting from room temperature. After the target temperature was reached the temperature was hold for 10 min until the Raman spectrum was taken. Subsequently the next temperature set point was addressed. Fig. 5 shows the molar flow rates of the reactants and the products as followed by online mass spectrometry. The reactor temperature set points are indicated by dotted vertical lines and the corresponding Raman spectra were recorded at the dashed line positions. A plot of the G-band normalized Raman spectra is shown in Fig. 6.

At ambient temperature up to $300 \text{ }^\circ\text{C}$ no reaction was observed as indicated by the constant reactant molar flow rates. No product species were detected. The recorded Raman spectra in this temperature range showed no significant differences in comparison to the clean platinum foil after oxidative and reductive treatment. At a reactor temperature of $400 \text{ }^\circ\text{C}$ the oxygen molar flow rate decreased barely visible indicating a beginning of reaction. Water and carbon dioxide are the exclusive reaction products at $400 \text{ }^\circ\text{C}$. The minor reactivity detected by the mass spectrometer did not lead to any changes in the Raman spectrum at this temperature, it was still the same as for the clean platinum foil.

Reaction light-off occurred during heating to $500 \text{ }^\circ\text{C}$. The methane molar flow rate decreased in a step-like manner under total consumption of oxygen. The reaction products at $500 \text{ }^\circ\text{C}$ were that of methane combustion CO_2 and H_2O with only traces of CO being formed. Hydrogen was not yet detected at this temperature. From the catalytic data (Fig. 5) it can be seen that the reactant and product molar flow rates stayed approximately constant after the first 10 min upon reaching the next temperature level. In the Raman spectrum the carbon region changed dramatically after reaction light-off, now showing the typical broad and strongly overlapping carbon peaks as described in detail in Section 3.1. As outlined in the introduction this carbon formation could block/passivate parts of the active Pt centers in methane CPO explaining why methane CPO on α -alumina supported platinum catalysts is slower than on the corresponding Rh catalysts operating in film transport regime. However this is a hypothesis at the moment as the experimental confirmation on α -alumina supported platinum foam catalysts is still due.

If the temperature was further increased to $600 \text{ }^\circ\text{C}$ carbon monoxide and hydrogen were formed in larger amounts. The reactivity plot in Fig. 5 shows a significant induction behavior of the methane CPO under this conditions. Immediately after the heating step to $600 \text{ }^\circ\text{C}$ the reactivity of the platinum foil is highest as indicated by the step-like increase in methane conversion and carbon monoxide and hydrogen formation. At the same time the molar flow rates of carbon dioxide and water show a mirror like decrease. This initial activity decays then asymptotically to the new steady state activity. For the temperature step to $700 \text{ }^\circ\text{C}$ the same response is observed. Immediately after the temperature increase, methane conversion and synthesis gas selectivities are highest but decrease towards a new steady state. Upon switching to $800 \text{ }^\circ\text{C}$ the induction period is lost and the new steady state is almost immediately reached.

Fig. 6 shows the corresponding Raman spectra recorded at each temperature set point and Table 1 summarizes the fitting parameters according to Sadezky et al. [12]. As discussed in Section 3.1 the D1 FWHM together with the D3 band intensity can be used as indicators for the chemical nature of carbonaceous materials allowing discrimination between different defective carbon species. Fig. 6 shows clearly that the carbon species formed on the platinum surface change their structure significantly as a function of reaction temperature. The D3 band intensity decreased by one fourth of its initial value by increasing the temperature from 500 to $800 \text{ }^\circ\text{C}$. Simultaneously the D1 FWHM is reduced by more than 20 %. This is a direct evidence for a steady loss in the amorphous molecular carbon fraction and increasing structural order of the initially amorphous coke deposits with increasing temperature. Furthermore the carbon Raman spectra show a pronounced change with time on stream. The dotted spectrum in Fig. 6 shows the state of the surface carbon after keeping the reactor temperature at $800 \text{ }^\circ\text{C}$ for additional 5.5 h under reaction conditions. The spectrum turns into an almost perfect graphite spectrum with two narrow bands at about ~ 1344 and $\sim 1567 \text{ cm}^{-1}$. Obviously, under the investigated conditions the highly reactive molecular carbon species are gasified either by oxidation or by methanation with time on stream from the Pt surface. Due to the totally defect controlled reactivity of carbon materials only unreactive, highly ordered carbon is left behind.

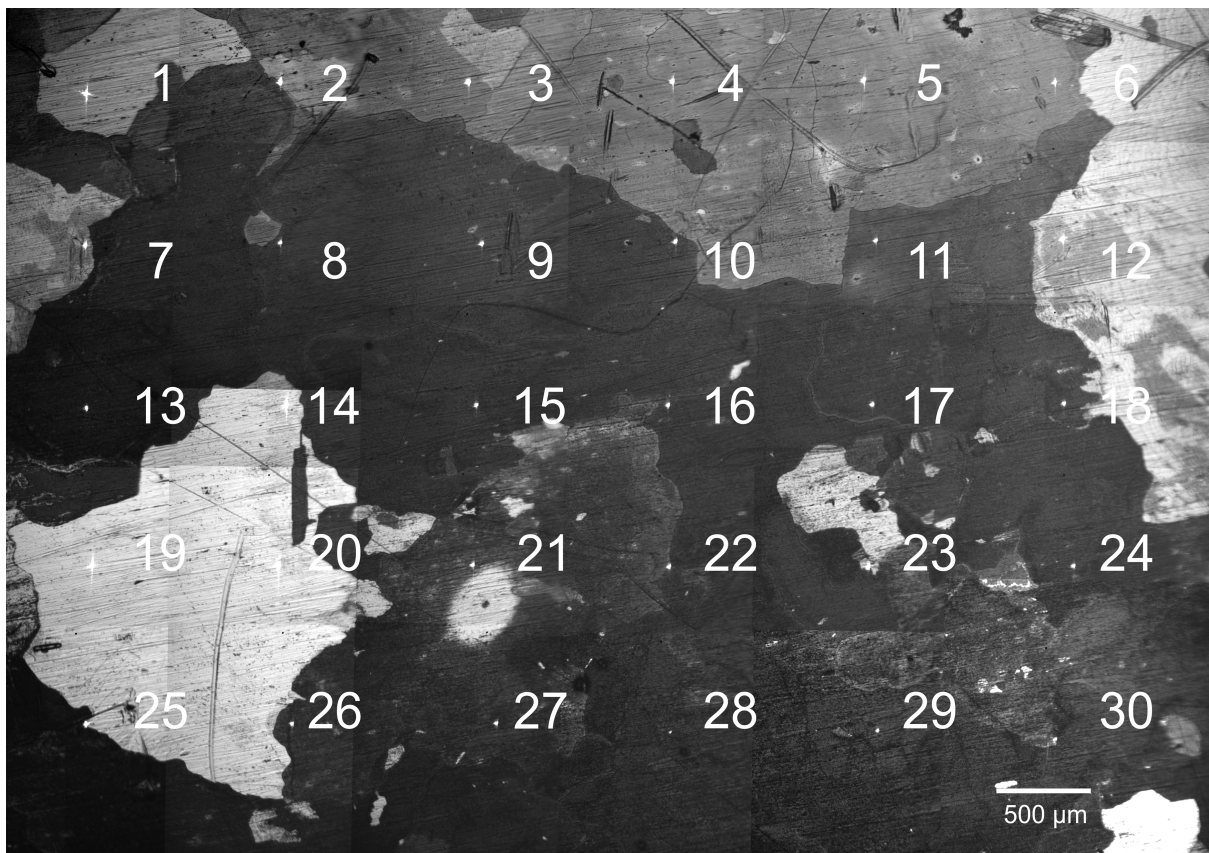
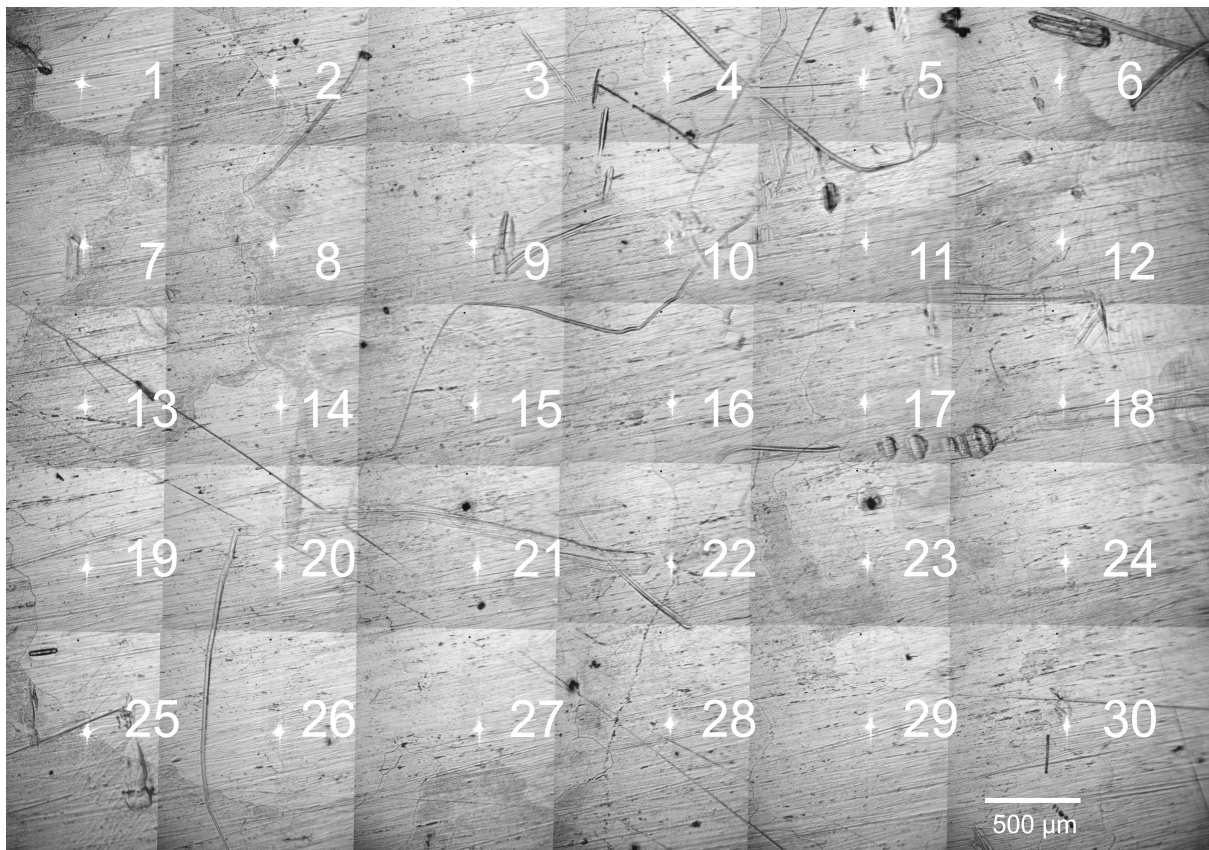


Figure 4: Light-optical micrograph of the polycrystalline platinum foil serving as model catalyst in methane CPO. The bright laser spots indicate the Raman sampling positions. Top: Platinum foil after oxidative and reductive cleaning as described in Section 2. Bottom: Platinum foil under CPO conditions at $T = 800\text{ }^{\circ}\text{C}$ reactor cell temperature.

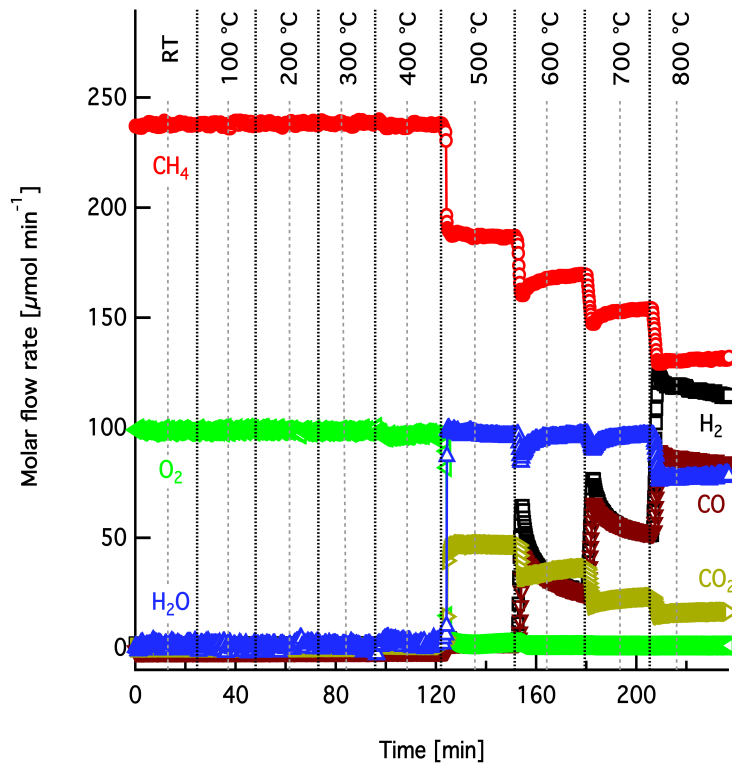


Figure 5: Molar flow rates of reactants and products during temperature programmed methane CPO. Dotted lines indicate reactor temperature set points. Dashed lines indicate time coordinates where a corresponding Raman spectra was recorded.

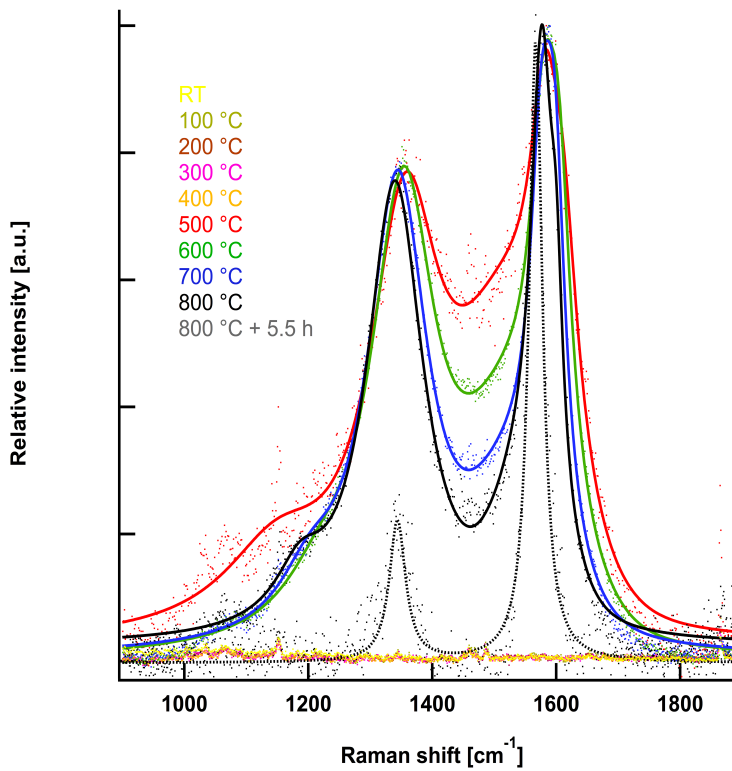


Figure 6: Evolution of carbon Raman bands as function of reactor cell temperature. Dots: normalized measured Raman intensity, lines: fit according to Sadezky et al. [12].

Table 1: Fitting parameters for quantitative spectral analysis of carbon Raman bands formed during temperature programmed methane CPO on a platinum foil according to the five band fitting procedure proposed by Sadezky et al. [12].

T [°C]	D4 pos. [cm ⁻¹]	D4 FWHM [cm ⁻¹]	D4 area [a.u.]	D1 pos. [cm ⁻¹]	D1 FWHM [cm ⁻¹]	D1 area [a.u.]	D3 pos. [cm ⁻¹]	D3 FWHM [cm ⁻¹]
RT-400	—	—	—	—	—	—	—	—
500	1149	211.5	41.4	1356	142.5	149.9	1528	187.5
600	1221	144.8	16.0	1354	129.8	149.9	1536	179.6
700	1203	119.0	14.9	1345	120.0	140.2	1536	154.7
800	1187	96.7	12.1	1340	111.1	125.5	1550	116.2
800	—	—	—	1344	31.6	11.1	—	—

T [°C]	D3 area [a.u.]	G pos. [cm ⁻¹]	G FWHM [cm ⁻¹]	G area [a.u.]	D2 pos. [cm ⁻¹]	D2 FWHM [cm ⁻¹]	D2 area [a.u.]
RT-400	—	—	—	—	—	—	—
500	80.5	1581	57.3	34.6	1612	60.9	30.7
600	57.7	1579	50.7	35.4	1605	48.0	31.9
700	33.4	1576	44.5	34.1	1598	41.1	31.8
800	21.6	1577	42.5	48.7	1600	25.0	10.6
800	—	1567	26.0	40.0	—	—	—

4 In-situ Raman x,y-Mapping of Platinum Foil During Methane CPO

To confirm the observations described above and obtain a more generalized picture of the platinum foil, a 6 x 5 grid of sampling points was selected to cover the entire Pt foil uniformly. Fig. 4 enumerates the sampling positions indicated by the bright laser dots in the displayed composite light-optical micrographs.

The clean platinum foil was heated to 800 °C reactor temperature with 50 K min⁻¹ under a constant gas feed of $\dot{V}_{Ar}/\dot{V}_{CH_4}/\dot{V}_{O_2} = 11.73/11.42/2.84$ mln min⁻¹ respectively corresponding to a C/O ratio of 2.0. After about ~ 16 min the final reactor cell temperature was reached where the Pt foil was hold for another 30 min time on stream before the first Raman spectrum was measured at sampling position 1. After the first spectrum was taken all other positions were addressed successively by computer controlled movement of the reactor cell mounted on the x, y, z microscope table under the fixed laser focus. Fig. 7 shows the molar flow rates of reactant and products measured by online mass spectrometry during the mapping experiment. After reaction light-off oxygen is fully consumed but the initial high methane conversion decreased quickly within the first ~ 10 min accompanied by a decrease in all product flow rates. With further time on stream the flow rates of H₂, CO increase slightly before they reach steady state at about ~ 3 h time on stream. The first Raman spectrum (position 1) was recorded after the strong initial reactivity changes had leveled off. Prior measuring of the Raman spectra a light-optical micrograph was recorded at each sampling position. The right panel of Fig. 4 depicts a superposition of all sampling positions during the mapping experiment together with a panoramic view of the entire foil. Already from the light-optical micrograph the coke deposits covering the platinum foil can be identified. Remarkably, the surface is not evenly covered by carbon deposits but rather distinct zones of higher and lower gray contrast can be discriminated, which are separated by sharp boundaries. By their size and shape these zones can be assigned to the randomly oriented crystallites forming the foil microstructure. Generally, highly graphitized carbon species can be identified. Most of the sampling positions resemble each other and exhibit two sharp carbon bands, located at about ~ 1344 (D1) and ~ 1567 cm⁻¹ (G). The blue trace in Fig. 8, left panel, recorded at sampling position 15 represents this most common peak shape. The right graph in Fig. 8 shows the relative D band intensity ((D1 area)/(G area) or (D4+D1 area)/(G+D2 area)) as a function of the gray level in the light-optical micrographs from Fig. 4 and allows discrimination between sampling positions with different spectral information. The majority of sampling points concentrate at a relative D intensity around 0.5 or smaller and medium to dark gray level. Deviations from the average spectral shape and therefore position in Fig. 8 will be highlighted in the following.

Position one and two are apparently covered by the defect richest carbon which is in line with the results discussed earlier showing that amorphous and inhomogeneous carbon species are formed after reaction light-off. The black trace in Fig. 8 shows the Raman spectrum recorded at position one. The peak shape is broader than all other spectra and D and G band are strongly overlapping. The G band maximum is significantly shifted to higher wavenumbers compared to all other spectra due to a rather high D2 band intensity. In the Raman spectrum measured at position two a shoulder to the G band can still be discerned but much less pronounced than at position one. With longer time on stream the rather reactive amorphous carbon is being removed from the surface or converted into an oxidation resistant highly ordered planar carbon. For all spectra measured later than position two the five band fitting procedure suggested by Sadezky and coworkers [12] does no longer lead to converging results due to the graphite-like nature of the carbon surface species. It can therefore be estimated that the structural changes of the initial carbon species are largely finished within 1 h after reaction light-off.

Positions 7, 14, and 25 gave Raman spectra of significantly lower signal intensity as can be seen in Fig. 8 on the lower signal to noise ratio, represented by the green trace in Fig. 8 (left panel). Even though the intensity of a Raman band cannot be easily correlated with the surface concentration of a particular species, it can be assumed the the amount of surface carbon is less than for the other sampling positions in agreement with the gray contrast observed in the light-optical micrograph (Fig. 4, right panel).

Position 19 and 20 attract particular attention (represented by red trace in Fig. 8, left panel), because they do not exhibit any detectable carbon bands. Also the crystallite that is probed at these positions looks rather metallic in the light-optical micrograph. This is an remarkable finding which has important consequences for the microkinetic modeling of such reactions in which all catalytic sites are always treated alike which is called the ‘mean field approach’ [8, 10].

The origin of this interesting phenomenon can not be explained so far and needs further investigation. But the fact that some foil domains coke strong and some do not or weaker suggests that the reaction is structure sensitive. It is well known from surface science literature that the activity for breaking H–H, C–H, and C–C bonds is controlled by surface irregularities, steps, and kinks. Their abundance and accessibility direct the selectivity and activity in hydrocarbon conversion. Dehydrogenation reactions on Pt are controlled by the step density of a Pt single crystal surface [23]. The step density is determined by the angle and orientation

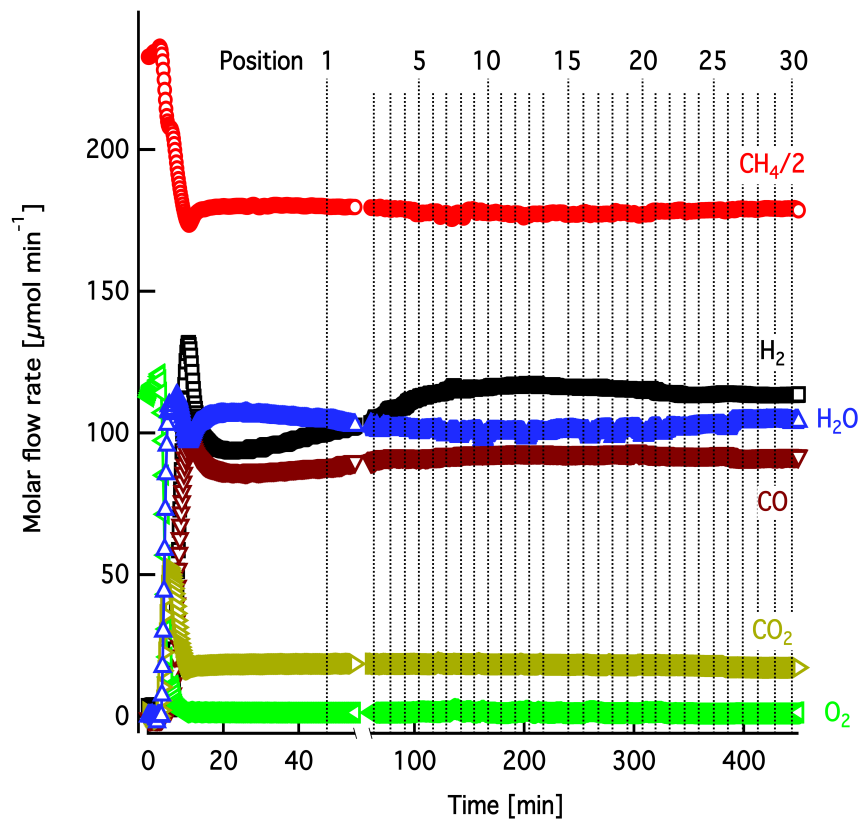


Figure 7: Reactant and product molar flow rates measured during the in-situ Raman mapping experiment under methane CPO conditions. Dotted vertical lines indicate the time coordinate where Raman spectra were recorded. Positions correlate with Fig. 4.

of the crystal phase. For this reason the observed inhomogeneous carbon distribution could reflect domains with higher and lower step density, respectively reactivity. Furthermore surface additives are influencing the working catalyst. These additives are deposited reversibly or irreversibly by the catalyst pretreatment, by the reaction mixture under the conditions of reaction, by addition of a promotor, or by migration of bulk impurities to the surface. A contamination from the reactor cell itself can cause surface additives, too. These add species may also cause structural reconstruction or subsurface chemistry.

5 Conclusions

The results presented in this paper give evidence for a substantial formation of surface carbon in methane CPO over a polycrystalline platinum foil. Using in-situ Raman spectroscopy and spectral analysis by curve fitting with five first-order Raman bands (G, D1, D2, D3, D4) according to [12], formation, evolution and nature of surface carbon could be characterized. Highly defective and inhomogeneous carbonaceous compounds are directly formed after reaction light-off and transformed into ordered graphite-like species. This transformation occurs on a timescale of several ten minutes up to approximately one hour. The carbon distribution at the Pt surface was found to be inhomogeneous and somehow related to the nature of the micro-crystals making up the polycrystalline Pt foil. The exact origin of this unisotropy is not yet understood and needs further systematic investigation. The blockage of Pt surface sites by oxidation resistant graphitic carbon could be the reason why methane CPO on Pt proceeds much slower and with poorer synthesis gas selectivity compared to Rh which operates reportedly in a film transport limited regime at low surface coverage. With respect to literature published on microkinetic modeling of methane CPO on Pt (e.g. [24,25]) it can be concluded that these models have to be revised as they predict an empty Pt surface under methane CPO conditions and do neither consider multilayer carbon formation on the Pt surface nor the inhomogeneities observed in the present study.

Acknowledgements

All authors thank the German Research Foundation for funding the Emmy-Noether-Junior-Research-Group "High Temperature Catalysis". Further support was provided by the German Federal Ministry of Education and Research within the framework of the Excellence Cluster "Unifying Concepts in Catalysis".

References

- [1] D. A. Hickman, L. D. Schmidt, Production of Syngas by Direct Catalytic Oxidation of Methane, *Science* 259 (5093) (1993) 343–346. doi:10.1126/science.259.5093.343.
- [2] D. A. Hickman, L. D. Schmidt, Steps in CH₄ Oxidation on Pt and Rh Surfaces: High-Temperature Reactor Simulations, *AIChE J.* 39 (7) (1993) 1164–1177. doi:10.1002/aic.690390708.
- [3] D. A. Hickman, E. A. Hauptfear, L. D. Schmidt, Synthesis gas formation by direct oxidation of methane over Rh monoliths, *Catal. Lett.* 17 (3-4) (1993) 223–237. doi:10.1007/BF00766145.
- [4] D. A. Hickman, L. D. Schmidt, Synthesis Gas Formation by Direct Oxidation of Methane over Monoliths, *ACS Symp. Ser.* 523 (1993) 416–426. doi:10.1021/bk-1993-0523.ch032.
- [5] R. Horn, K. A. Williams, N. J. Degenstein, A. Bitsch-Larsen, D. Dalle Nogare, S. A. Tupy, L. D. Schmidt, Methane catalytic partial oxidation on autothermal Rh and Pt foam catalysts: Oxidation and reforming zones, transport effects, and approach to thermodynamic equilibrium, *J. Catal.* 249 (2) (2007) 380–393. doi:10.1016/j.jcat.2007.05.011.
- [6] A. P. E. York, T. Xiao, M. L. H. Green, Brief Overview of the Partial Oxidation of Methane to Synthesis Gas, *Top. Catal.* 22 (3-4) (2003) 345–358. doi:10.1023/A:1023552709642.
- [7] A. Bitsch-Larsen, R. Horn, L. D. Schmidt, Catalytic partial oxidation of methane on rhodium and platinum: Spatial profiles at elevated pressure, *Appl. Catal., A* 348 (2) (2008) 165–172. doi:10.1016/j.apcata.2008.06.036.
- [8] D. Dalle Nogare, N. J. Degenstein, R. Horn, P. Canu, L. D. Schmidt, Modeling spatially resolved profiles of methane partial oxidation on a Rh foam catalyst with detailed chemistry, *J. Catal.* 258 (1) (2008) 131–142. doi:10.1016/j.jcat.2008.06.006.

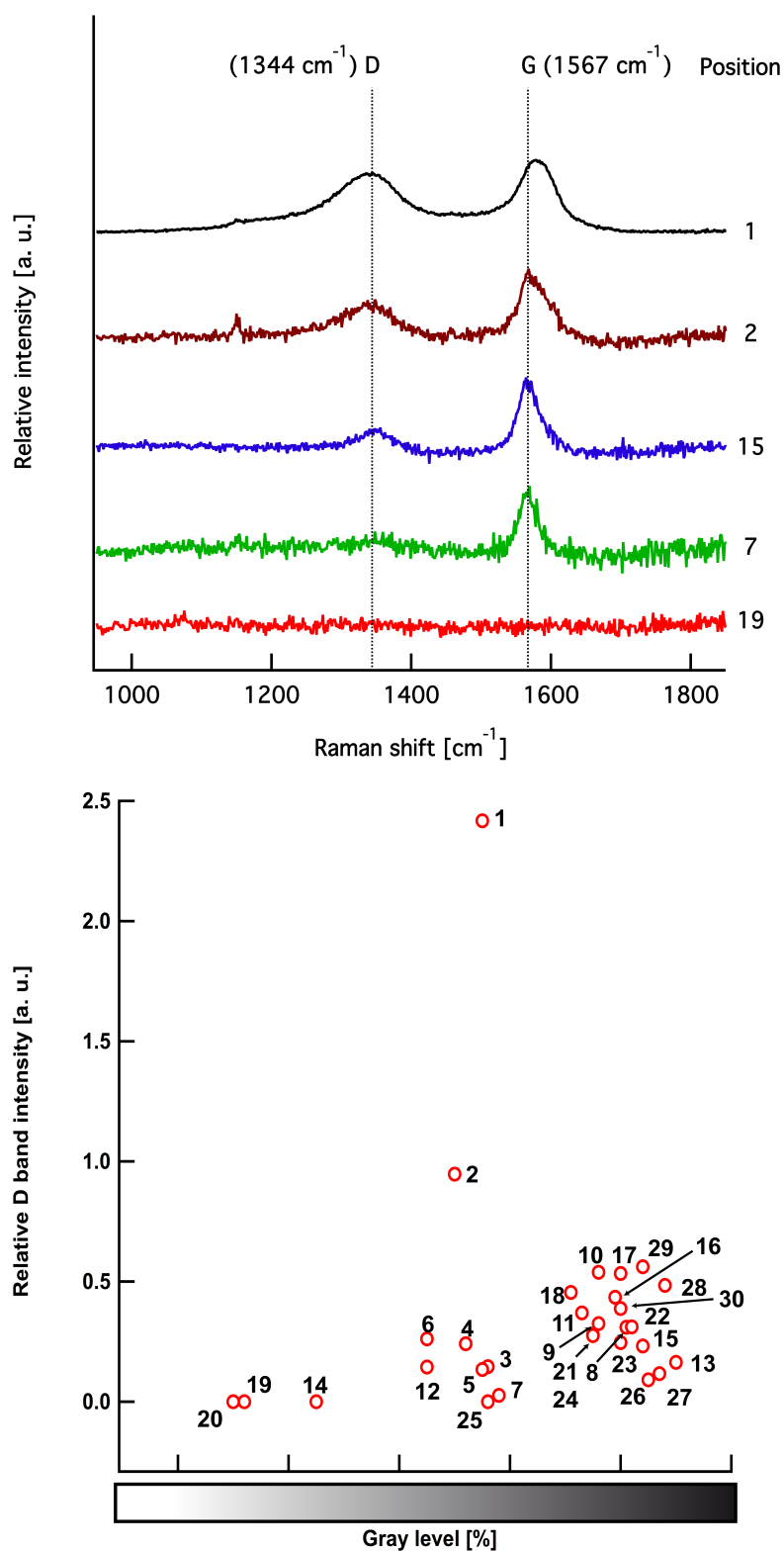


Figure 8: Top: Selected in-situ Raman spectra recorded during methane CPO on a polycrystalline platinum foil. Spectra are normalized to the G band maximum for better comparability. Bottom: Cloud plot of relative D band intensity as a function of observed gray level in the light-optical micrographs of Fig. 4 right. Positions correlate with Fig. 4.

- [9] D. Dalle Nogare, N. J. Degenstein, R. Horn, P. Canu, L. D. Schmidt, Modeling Spatially Resolved Data of Methane Catalytic Partial Oxidation on Rh Foam Catalyst at Different Inlet Compositions and Flow Rates, *J. Catal.* 277 (2) (2011) 134–148. doi:10.1016/j.jcat.2010.10.020.
- [10] A. Donazzi, M. Maestri, B. C. Michel, A. Beretta, P. Forzatti, G. Groppi, E. Tronconi, L. D. Schmidt, D. G. Vlachos, Microkinetic Modeling of Spatially Resolved Autothermal CH_4 Catalytic Partial Oxidation Experiments over *Rh*-coated Foams., *J. Catal.* 275 (2010) 270–279. doi:10.1016/j.jcat.2010.08.007.
- [11] I. B. Gornushkin, P. E. Eagan, A. B. Novikov, B. W. Smith, J. D. Winefordner, Automatic Correction of Continuum Background in Laser-Induced Breakdown and Raman Spectrometry, *Appl. Spectrosc.* 57 (2) (2003) 197–207.
URL <http://www.opticsinfobase.org/abstract.cfm?URI=as-57-2-197>
- [12] A. Sadezky, H. Muckenhuber, H. Grothe, R. Niessner, U. Pöschl, Raman microspectroscopy of soot and related carbonaceous materials: Spectral analysis and structural information, *Carbon* 43 (5) (2005) 1731–1742. doi:10.1016/j.carbon.2005.02.018.
- [13] A. C. Ferrari, J. Robertson, Interpretation of Raman spectra of disordered and amorphous carbon, *Phys. Rev. B* 61 (20) (2000) 14095–14107. doi:10.1103/PhysRevB.61.14095.
- [14] F. Tuinstra, J. L. Koenig, Raman Spectrum of Graphite, *J. Phys. Chem.* 53 (3) (1970) 1126–1130. doi:10.1063/1.1674108.
- [15] G. Katagiri, H. Ishida, A. Ishitani, Raman spectra of graphite edge planes, *Carbon* 26 (4) (1988) 565–571. doi:10.1016/0008-6223(88)90157-1.
- [16] Y. Wang, D. C. Alsmeyer, R. L. McCreery, Raman spectroscopy of carbon materials: structural basis of observed spectra, *Chem. Mater.* 2 (5) (1990) 557–563. doi:10.1021/cm00011a018.
- [17] N. P. Ivleva, U. McKeon, R. Niessner, U. Pöschl, Raman Microspectroscopic Analysis of Size-Resolved Atmospheric Aerosol Particle Samples Collected with an ELPI: Soot, Humic-Like Substances, and Inorganic Compounds, *Aerosol Sci. Technol.* 41 (7) (2007) 655–671. doi:10.1080/02786820701376391.
- [18] M. Knauer, M. E. Schuster, D. Su, R. Schlögl, R. Niessner, N. P. Ivleva, Soot Structure and Reactivity Analysis by Raman Microspectroscopy, Temperature-Programmed Oxidation, and High-Resolution Transmission Electron Microscopy, *J. Phys. Chem. A* 113 (50) (2009) 13871–13880. doi:10.1021/jp905639d.
- [19] B. Dippel, H. Jander, J. Heintzenberg, NIR FT Raman spectroscopic study of flame soot, *Phys. Chem. Chem. Phys.* 1 (1999) 4707–4712. doi:10.1039/A904529E.
- [20] B. Dippel, J. Heintzenberg, Soot characterization in atmospheric particles from different sources by NIR FT Raman spectroscopy, *J. Aerosol Sci.* 30 (1999) S907–S908. doi:10.1016/S0021-8502(99)80464-9.
- [21] A. Cuesta, P. Dhamelincourt, J. Laureyns, A. Martínez-Alonso, J. M. D. Tascón, Raman microprobe studies on carbon materials, *Carbon* 32 (8) (1994) 1523–1532. doi:10.1016/0008-6223(94)90148-1.
- [22] T. Jawhari, A. Roid, J. Casado, Raman spectroscopic characterization of some commercially available carbon black materials, *Carbon* 33 (11) (1995) 1561–1565. doi:10.1016/0008-6223(94)90148-1.
- [23] G. A. Somorjai, *Chemistry in Two Dimensions: Surfaces*, Cornell University Press, Ithaca and London, 1981, Ch. 9. Hydrocarbon Conversion on Platinum, pp. 479–515.
- [24] A. B. Mhadeshwar, D. G. Vlachos, A Catalytic Reaction Mechanism for Methane Partial Oxidation at Short Contact Times, Reforming, and Combustion, and for Oxygenate Decomposition and Oxidation on Platinum., *Ind. Eng. Chem. Res.* 46 (16) (2007) 5310–5324. doi:10.1021/ie070322c.
- [25] R. Quiceno, J. Pérez-Ramírez, J. Warnatz, O. Deutschmann, Modeling the high-temperature catalytic partial oxidation of methane over platinum gauze: Detailed gas-phase and surface chemistries coupled with 3D flow field simulations, *Appl. Catal., A* 303 (2006) 166–176. doi:10.1016/j.apcata.2006.01.041.